

Supporting Information for

Ultrasensitive Vertical Piezotronic Transistor based on ZnO Twin Nanoplatelet

Longfei Wang¹, Shuhai Liu², Xiaolong Feng³, Qi Xu⁴, Suo Bai⁴, Laipan Zhu¹, Libo Chen¹, Yong Qin^{2} and
Zhong Lin Wang^{1,5*}*

¹Beijing Institute of Nanoenergy and Nanosystems, Chinese Academy of Sciences; National Center for
Nanoscience and Technology (NCNST), Beijing 100083, China

²School of Advanced Materials and Nanotechnology, Xidian University, 710071, China

³Microsystems and Terahertz Research Center, China Academy of Engineering Physics, Chengdu, Sichuan
610200, China

⁴Institute of Nanoscience and Nanotechnology, School of Physical Science and Technology, Lanzhou
University, Gansu 730000, China

⁵School of Material Science and Engineering, Georgia Institute of Technology, Atlanta, Georgia 30332,
United States

* Corresponding author. E-mail: zhong.wang@mse.gatech.edu, qinyong@lzu.edu.cn

This word file includes:

Materials and Methods

Supplementary Notes

Figure. S1 to S15

Table S1 to S2

References

Table of Contents

Materials and Methods.

1. Schematic of the experiment setup and contacts in the measurements.
2. Electronic transport property of the TNPT under Schottky effect.
3. Transport characteristics of TNPT devices with single Schottky junction.
4. Why we use the ‘Pressure sensitivity (meV/MPa)’, but not the ‘Force sensitivity (meV/nN)’?
5. Simulation of modulate effect of strain-induced piezo-potential on metal-ZnO Schottky barrier
6. Photoresponse of the ZnO twin nanoplatelet based photodetector.

Figure S1 to S15

Table S1. Summary of piezoelectric coefficients from different materials.

Table S2. A comparison of strain sensing works.

References

MATERIALS AND METHODS

Synthesis of ZnO twin nanoplatelets. In a typical synthesis, 30 ml aqueous solution containing 91 mM $\text{Zn}(\text{CH}_3\text{COO})_2$ and 151 mM Tris(hydroxymethyl)methyl aminomethane (THAM) was prepared in a glass container. The glass was then placed in an oven at 95 °C. ZnO twin nanoplatelets would appear in 2 h and could be collected for characterization and device fabrication.

Material characterizations

Detailed microscopic structures of ZnO twin nanoplatelets were characterized using scanning electron microscope (Hitachi SU8020), PANalytical X'Pert PRO diffractometer (Almelo, the Netherlands) with Cu KR radiation ($\lambda=0.15418$ nm) for X-ray diffraction patterns of the ZnO nanoplatelet and twin nanoplatelet. The effective piezoelectric coefficient d_{33} were measured by piezo-response force microscopy (PFM) (MFP-3D from Asylum Research).

Fabrication process of ZnO twin nanoplatelet-based piezotronic transistors

A 300 nm thick layer of SiO_2 by electron-beam evaporation was first coated over a heavily doped Si substrate. Then the substrate was coated with Cr/Au (5 nm/60 nm) by RF magnetron sputtering. Disperse a proper amount of ZnO twin nanoplatelets into ethanol under ultra-sonication for several minutes at room temperature to obtain homogeneous ethanol dispersion. Drop the ZnO twin nanoplatelet ethanol dispersion on the prepared substrate then blow-dry the substrates by compressed N_2 quickly. Repeat this procedure for several times.

Optical and electrical measurements of piezotronic (photo)transistor

I–V characteristics of the device were measured and recorded by using a conductive AFM system (Molecular Force Probe MFP-3D from Asylum Research) with a Pt coated Si AFM probe, which has a spring constant of 34.27 nN/nm and an inverse optical lever sensitivity (InvOLS) of 90.55 nm/V. The force applied to the TNPT was estimated by multiplying the spring constant, InvOLS and cantilever deflection. The optical input stimuli were provided by

a common Hg–Xe lamp (LC8-TLSX1046C03). A 365 nm optical filter was used to obtain the parallel UV light and UV filters were applied to achieve the various illumination intensities.

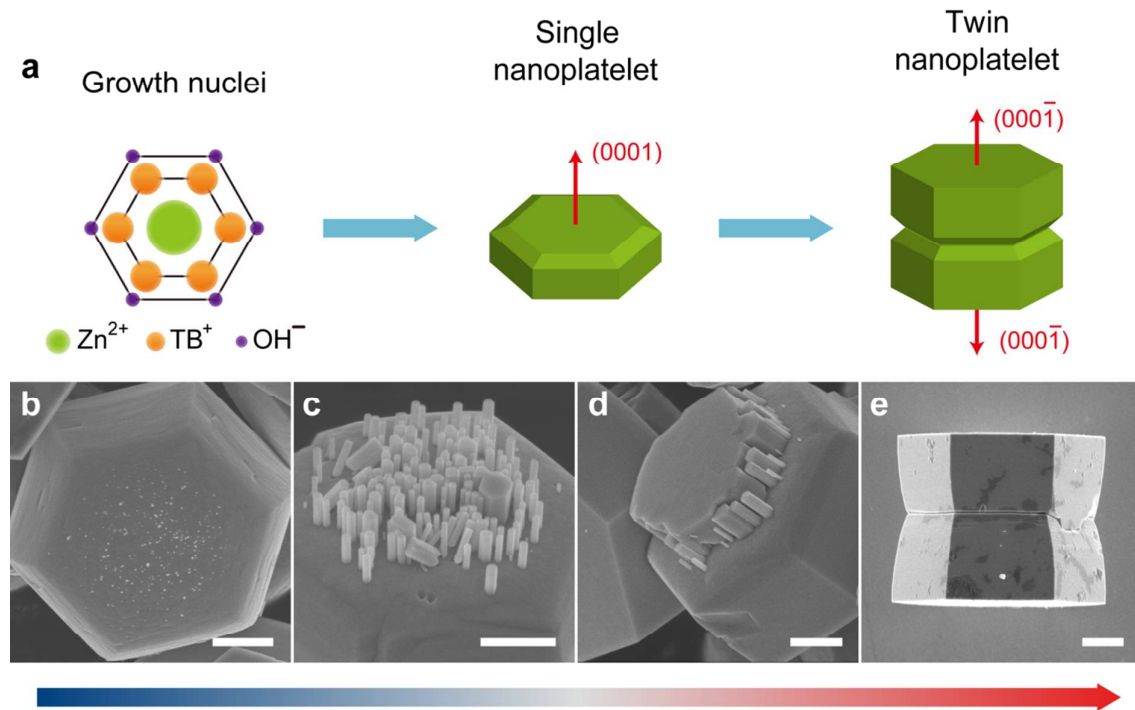


Figure S1. ZnO twin nanoplatelet design, synthesis and characterization. a) Schematic illustration of the synthesis of ZnO twin nanoplatelet structure. The nuclei are first formed on a single nanoplatelet, and then used as seed for the growth of twin nanoplatelet. b-e) The scanning electron microscopy (SEM) images show the ZnO nanoplatelet of different growth stages. The scale bar is 1 μm .

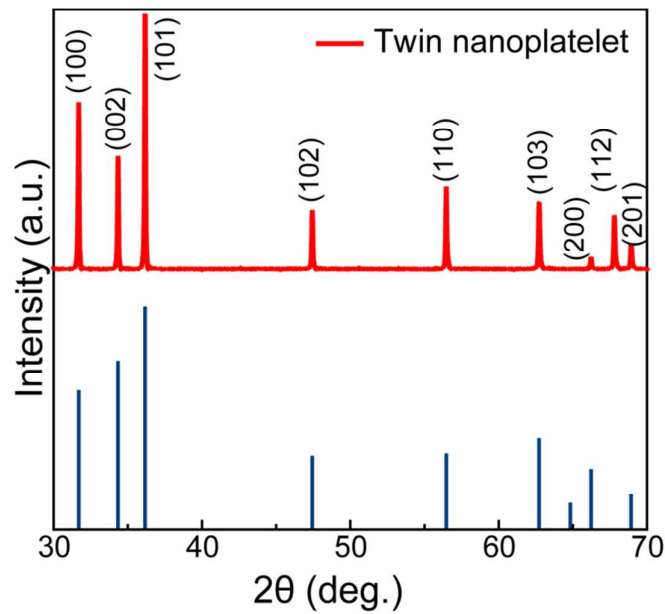


Figure S2. XRD pattern of ZnO twin nanoplatelet, which can be indexed to the wurtzite structure.

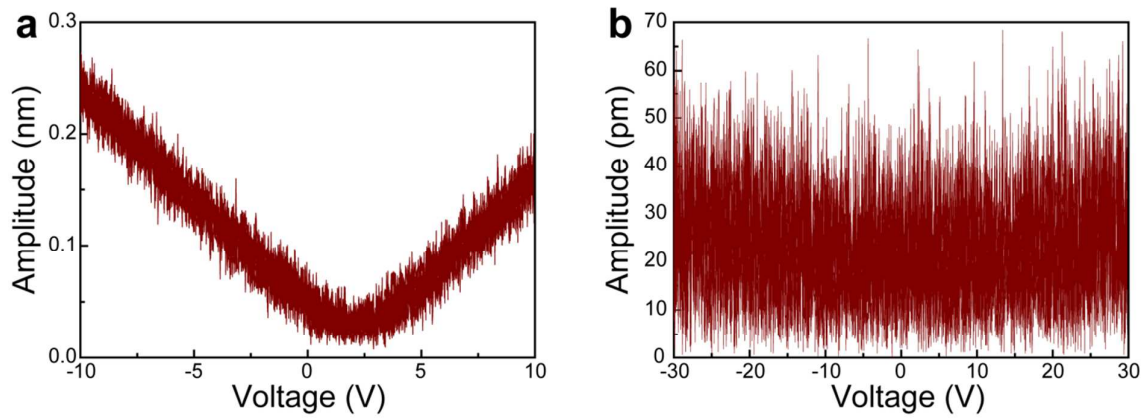


Figure S3. Piezoelectric coefficient d_{33} of ZnO single (a) and twin nanoplatelet (b) acquired under 1 Hz, which demonstrates ZnO nanoplatelet with high piezoelectric coefficient and the mirror symmetrical structure of twin nanoplatelet.

Table S1. Summary of piezoelectric coefficients from different materials.

Materials	Morphology	Piezo. Coefficient d_{33} (pm/V)	Reference
ZnO	Twin Nanoplatelet	0.25~0.68	This Work
ZnO	Nanoplatelet	18.9~22.5	(1)
ZnO	Bulk	~12.4	(2)
ZnO	Pillar	~7.5	(3)
ZnO	Nanorod	4.41 ± 1.73	(4)
ZnO	Nanobelt	0.4~9.5	(5)
ZnO	Nanobelt	14.3~26.7	(6)
GaN	Nanowire	~12.8	(7)
NaNbO ₃	Nanowire	0.85~4.26	(8)
KNbO ₃	Nanowire	~7.9	(9)
BaTiO ₃	Nanowire	~16.5	(10)

1. Schematic of the experiment setup and contacts in the measurements

The measurements were performed by AFM (Figure S4) using a Pt coated Si tip as the top electrode; while the Si/SiO₂ (300 nm) wafer planar substrate coated with Cr/Au film by magnetron sputtering was used as bottom electrode. The rectangular cantilever of tip has a calibrated normal spring constant of 34.27 nN/nm. There were two contacts in the measurements. One contact is between the Pt electrode and ZnO twin nanoplatelet, while the other is between ZnO twin nanoplatelet and Au electrode. Since the work function of Pt (5.65 eV) and Au (5.1 eV) are higher than the ZnO twin nanoplatelet's electron affinities (4.5 eV), the Pt-ZnO and ZnO-Au contact would be Schottky contact with an ideal Schottky barrier height (SBH).

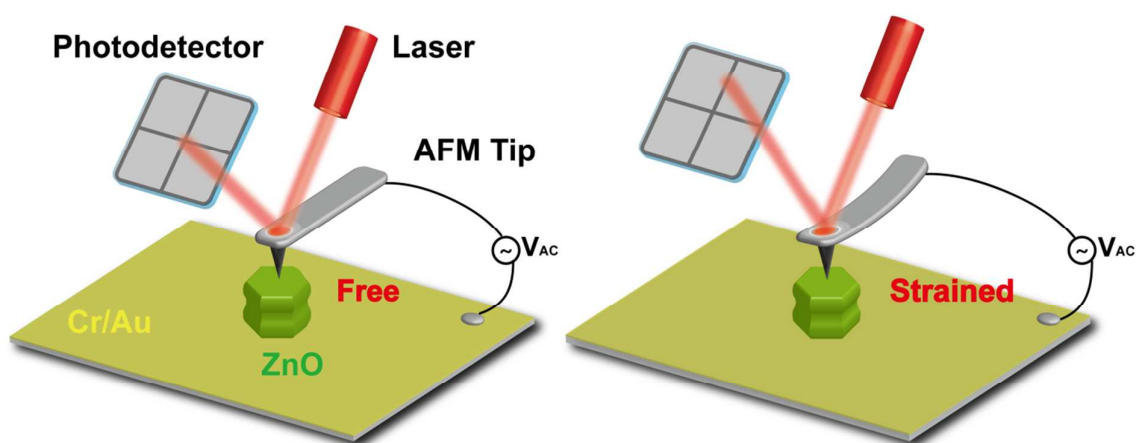


Figure S4. Schematic of the experiment setup for measuring the TNPT device. The ZnO twin nanoplatelet was vertical aligned on Au coated Si/SiO₂ wafer planar substrate. The measurements were performed by AFM using a Pt coated Si tip as the top electrode; while, the Si/SiO₂ (300 nm) wafer planar substrate coated with palladium (Au) film by magnetron sputtering was used as bottom electrode. The rectangular cantilever of tip had a calibrated normal spring constant of 34.27 nN/nm. The induced stress by AFM tip changed the load on the cantilever, which was observed by the deflection of a laser beam.

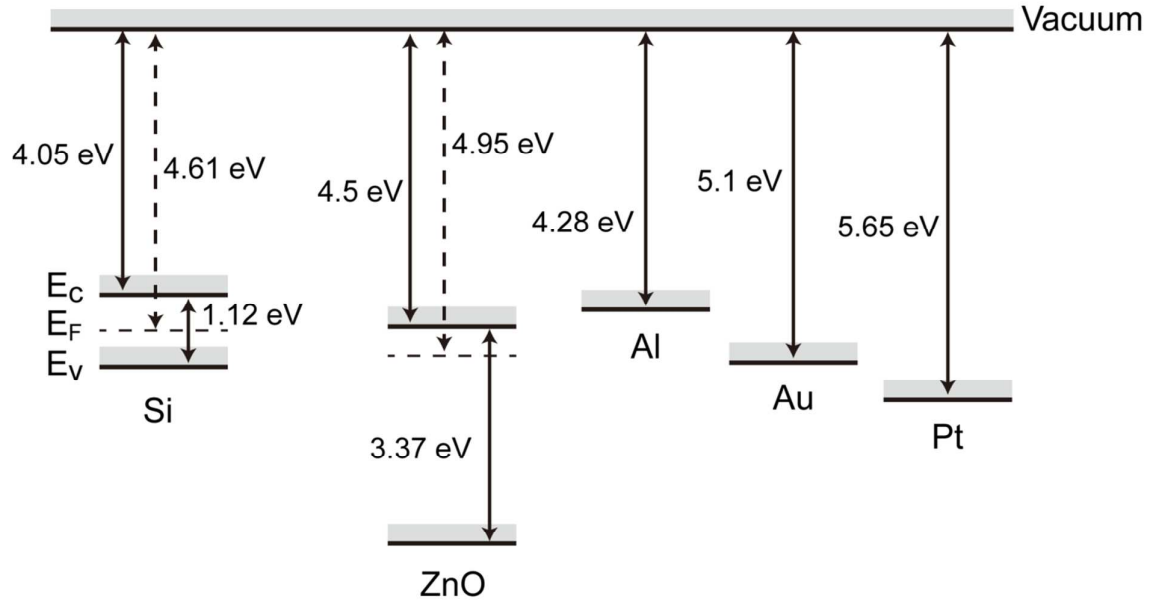


Figure S5. Electron affinity, work function and band gaps of Si, ZnO, Al, Au, and Pt used in the energy band diagrams.

2. Electronic transport property of TNPT under Schottky effect.

By considering the high doping concentrations of the ZnO twin nanoplatelet and all measurements were taken at room temperature, the thermionic-field-emission (TFE) models are most suitable for analyzing our experimental results. According to the classic thermionic emission-diffusion theory^{12, 13} (for $V \gg 3kT/q \sim 77$ mV) for a forward bias voltage V and at temperature T , the current through the forward biased I_F is

$$I_F \approx SA^*T^2 \exp\left(-\frac{q}{kT}\varphi_n\right) \exp\left(e\frac{q}{kT}V - 1\right) \quad (\text{S.1})$$

where S is the area of the Schottky contact, A^* is the effective Richardson constant, T is the absolute temperature, φ_n is the effective Schottky barrier height, k is the Boltzmann constant, q is the electron charge, and V is the applied voltage across the contact.

For a reversely biased n-type Schottky contact, according to the TFE theory, the current under reverse bias takes the form of

$$I_R \approx SJ_{sv} \exp\left(-\frac{q}{E_0} \varphi_n\right) \exp\left(V_R \left(\frac{q}{kT} - \frac{q}{E_0}\right)\right) \quad (\text{S.2})$$

Where, J_{sv} is the slowly varying term regarding applied voltage and Schottky barrier change, V_R is the reverse voltage, q is electron charge, k is the Boltzmann constant, and E_0 is a tunneling parameter of the same order of but larger than kT . Usually E_0 is larger than kT , and is constant regarding barrier height and applied voltage, so it is reasonable to assume that $E_0 = akT$, with $a > 1$, so equation (2) now becomes

$$I_R \approx SJ_{sv} \exp\left(-\frac{q}{akT} \varphi_n\right) \exp\left(V_R \frac{q}{kT} \left(1 - \frac{1}{a}\right)\right) \quad (\text{S.3})$$

The dependence of I on V under a fixed pressure can be written as

$$\ln I \propto V \quad (\text{S.4})$$

SBH changes calculation

Based on Schottky theory and previous reports,¹⁴ the calculated method of the strain-induced change of SBH ($\Delta\varphi_{piezo}$) can be derived as follows:

$$\begin{aligned} I &= SJ_{sv} e^{-\frac{\varphi_{Bn0} + \Delta\varphi_{piezo}}{kT}} \\ \Rightarrow I_{free} &= SJ_{sv} e^{-\frac{\varphi_{Bn0}}{kT}}, I_{strain} = SJ_{sv} e^{-\frac{\varphi_{Bn0} + \Delta\varphi_{piezo}}{kT}} \\ \Rightarrow \Delta\varphi_{piezo} &= -kT \ln(I_{strain} / I_{free}) \end{aligned} \quad (\text{S.5})$$

The $\Delta\varphi_{piezo}$ can be derived from the $\ln I$ - V plot at temperature T , and k is Boltzmann constant.

I_{strain} and I_{free} are the measuring current of ZnO twin nanoplatelet at a fixed bias with and without being strained, respectively. By this formula, we can obtain the magnitude of SBH changes under different strains as illustrated in Figure S6.

Electronic transport property of TNPT in forward bias model

Because of the the mirror symmetrical structure of ZnO twin nanoplatelet, the TNPT can also be effectively regulated by piezotronic effect in forward model. Theoretically, the transport characteristics of reverse bias and forward bias should be symmetrical under various pressures, which is different from that of piezotronic devices based on polar nanomaterial. Figure S7 show the $\ln(I) - V$ of TNPT in forward model, which is approximately linear and consistent with the piezotronic model. The SBH decreases with compressive strain as expected and the pressure sensitivity is ~ 1448.08 meV/Mpa. The difference of transport characteristics of TNPT in reverse model and forward model may be due to the asymmetric contacts (Pt-ZnO point contact and ZnO-Au surface contact) of the TNPT. The ZnO twin nanoplatelet-based piezotronic devices by utilizing the dual Schottky junction Synergistic regulation can be used for ultrasensitive pressure sensors, photodetectors *et al.*

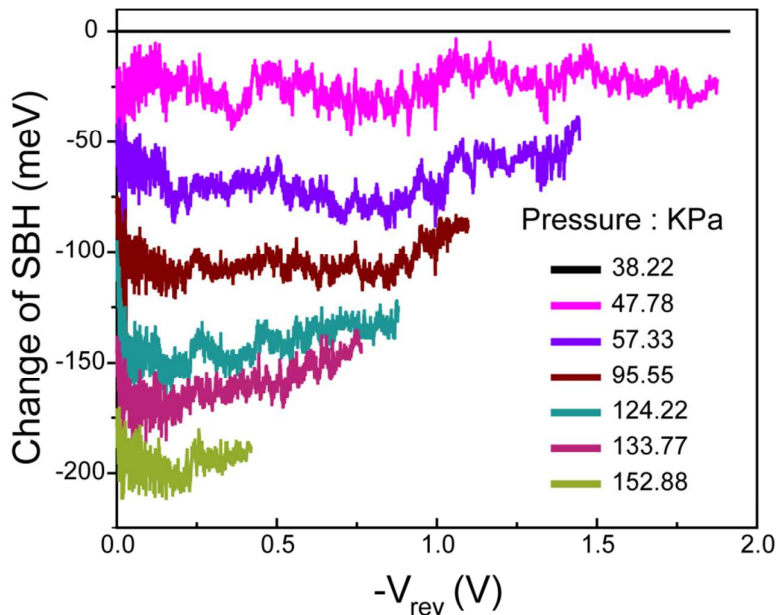


Figure S6. The magnitude of calculated Schottky barrier height (SBH) change as a function of the applied pressure under reverse bias condition.

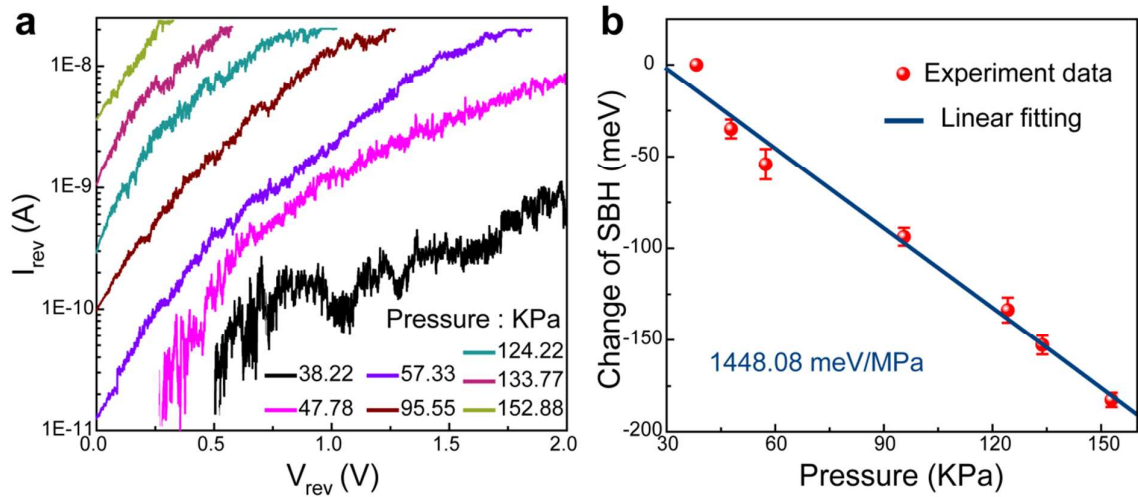


Figure S7. a) Current presented in semilog form vs voltage under forward bias condition. b) Calculated SBH change as a function of the applied pressure shows that the modulation effect of applied pressure on the SBH, demonstrating the extreme sensitivity of TNPT device. The dots are the experimented data and the blue line corresponds to the linear fitting function.

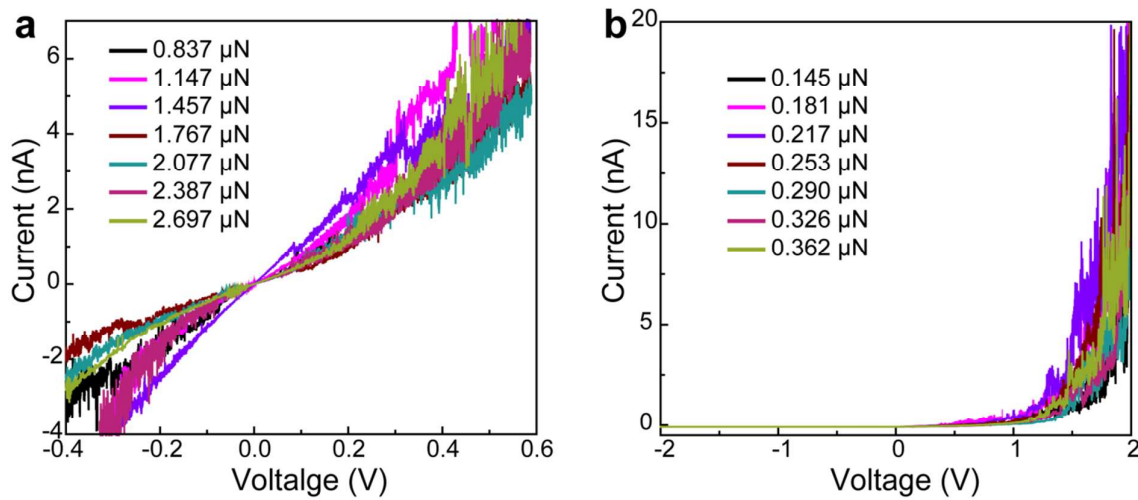


Figure S8. a) The pressure-independent I-V characteristics of the case that AFM Pt coated Si tip directly press on the Au bottom electrode. b) The pressure-independent I-V characteristics of the case that AFM n-Si tip directly press on the Au bottom electrode.

3. Transport characteristics of TNPT devices with single Schottky junction

In order to estimate the force sensitivities of Schottky junctions including AFM tip Pt-ZnO contact and substrate electrode Au-ZnO contact, the transport characteristics of TNPTs with n-Si/ZnO/Au structure (Figure S9) and Pt/ZnO/Al (work function of 4.28 eV) structure (Figure S10) were measured. After the electrons' thermal equilibration is reached, the conduction band discontinuity between ZnO twin nanoplatelet and n-Si tip is relative small due to the n-type doped ZnO synthesized by hydrothermal growth. Although there should exist a barrier with theoretical value of ~ 0.11 eV, an Ohm contact was obtained in our device with n-Si/ZnO/Au structure, so that the ZnO/Au Schottky junction plays a dominant role in regulating the performance of the device. The Ohm contact can also be formed between ZnO twin nanoplatelet and Al electrode, hence the Pt/ZnO Schottky junction would play a dominant role in regulating the performance of the device with Pt/ZnO/Al structure. The following is the detailed analysis. The four different situations were named as mode 1, mode 2, mode 3 and mode 4 (Figure S11). Here we use R_1 and R_2 to estimate the effective barrier height of Pt-ZnO contact under forward and reversed bias respectively; while R_3 and R_4 to Au-ZnO junction. We can find the bottom Schottky junction plays a dominant role in regulating the ZnO twin nanoplatelet piezotronic transistor. This was probably due to the asymmetry of Schottky contact area of TNPT device. Furthermore, the force sensitivities of forward biased Schottky junctions has also been made significant changes when the Al electrode was replaced by Au electrode, so that the forward biased Schottky junctions (R_2 and R_3) could also make a significant role in regulating the piezotronic transistor which is always ignored in previous studies.

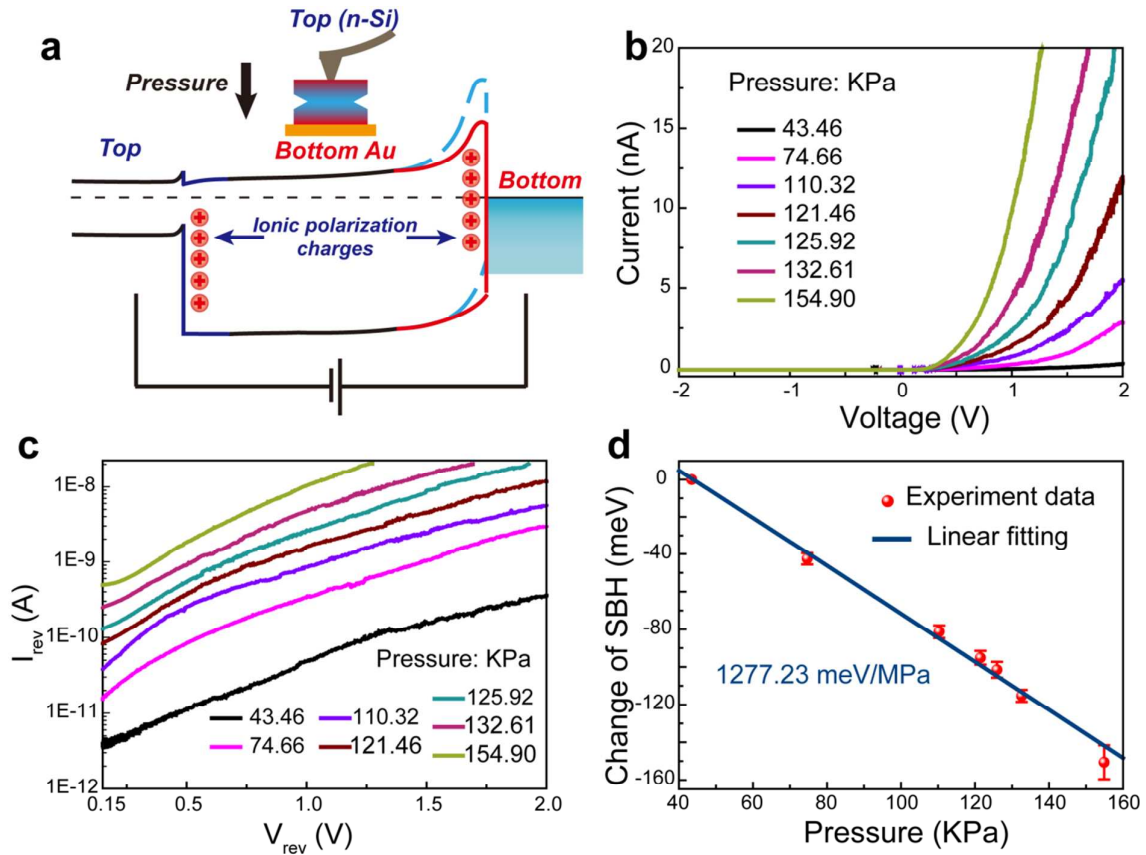


Figure S9. Transport characteristics of TNPT device with n-Si/ZnO/Au structure. The n-Si tip is pressed on the ZnO twin nanoplatelet, forming an Ohm contact between ZnO nanoplatelet and the top electrode. a) Band diagrams explaining the piezotronic behavior observed in a TNPT device as a result of the changes in Schottky barrier heights at Au-ZnO contact by strain-induced polarization charges. b) The modulation of carrier transport by strains under opposite drain bias in a TNPT device shows characteristic of a piezotronic effect. c) Current presented in semilog form vs voltage under forward bias condition indicates the transportation behavior at the forward-biased side is dominated by the forward-biased Schottky barrier. d) Calculated SBH change as a function of the applied pressure shows that the modulation effect of applied pressure on the SBH, demonstrating the extreme sensitivity of TNPT device. The dots are the experimented data and the blue line corresponds to the linear fitting function.

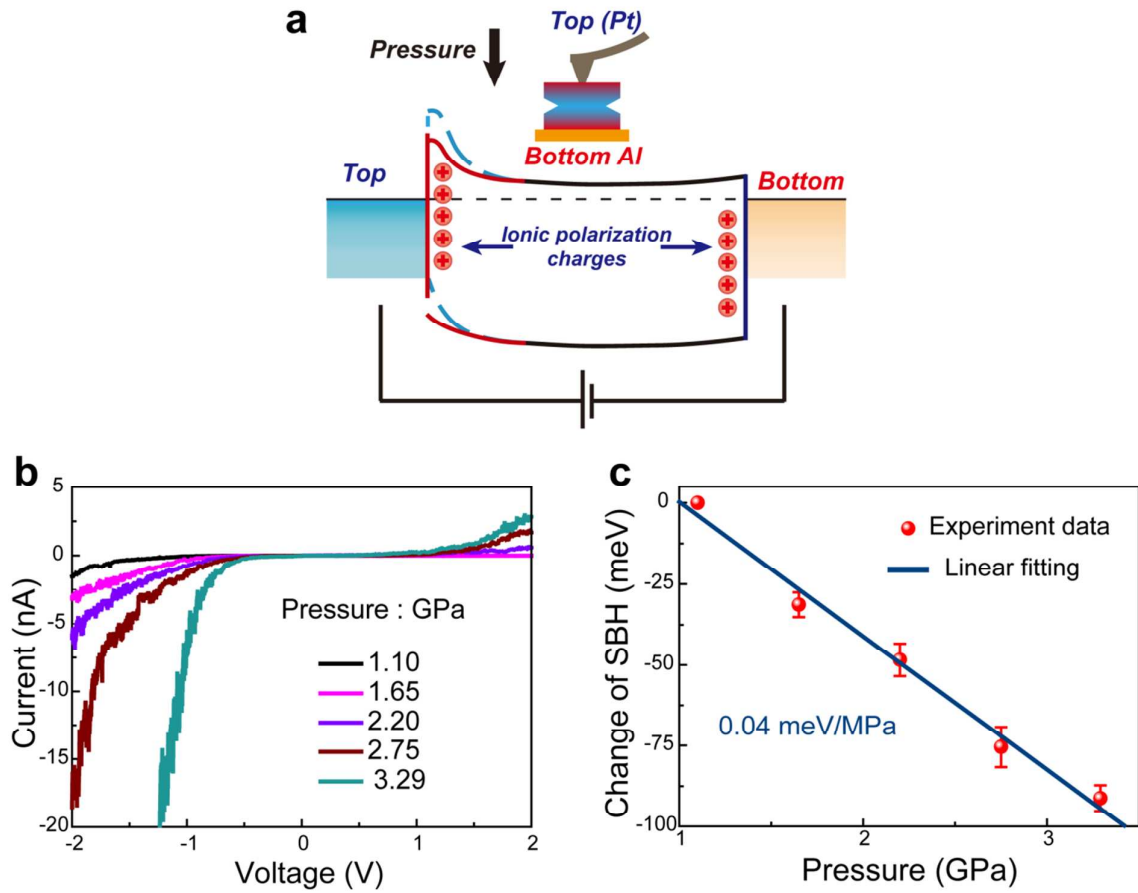


Figure S10. Transport characteristics of TNPT device with Pt/ZnO/Al structure. The ZnO twin nanoplatelet on the Si/SiO₂ wafer substrate coated with aluminum (Al) film as bottom electrode, forming an Ohm contact between ZnO twin nanoplatelet and the bottom electrode. a) Band diagrams explaining the piezotronic behavior observed in a TNPT device as a result of the changes in Schottky barrier heights at the Pt-ZnO contact by strain-induced positive polarization charges. b) The modulation of carrier transport by strains under opposite drain bias in a TNPT device shows characteristic of a piezotronic effect. c) Calculated SBH change as a function of the applied pressure shows that the modulation effect of applied pressure on the SBH, demonstrating the low sensitivity of TNPT device. The dots are the experimented data and the blue line corresponds to the linear fitting function.

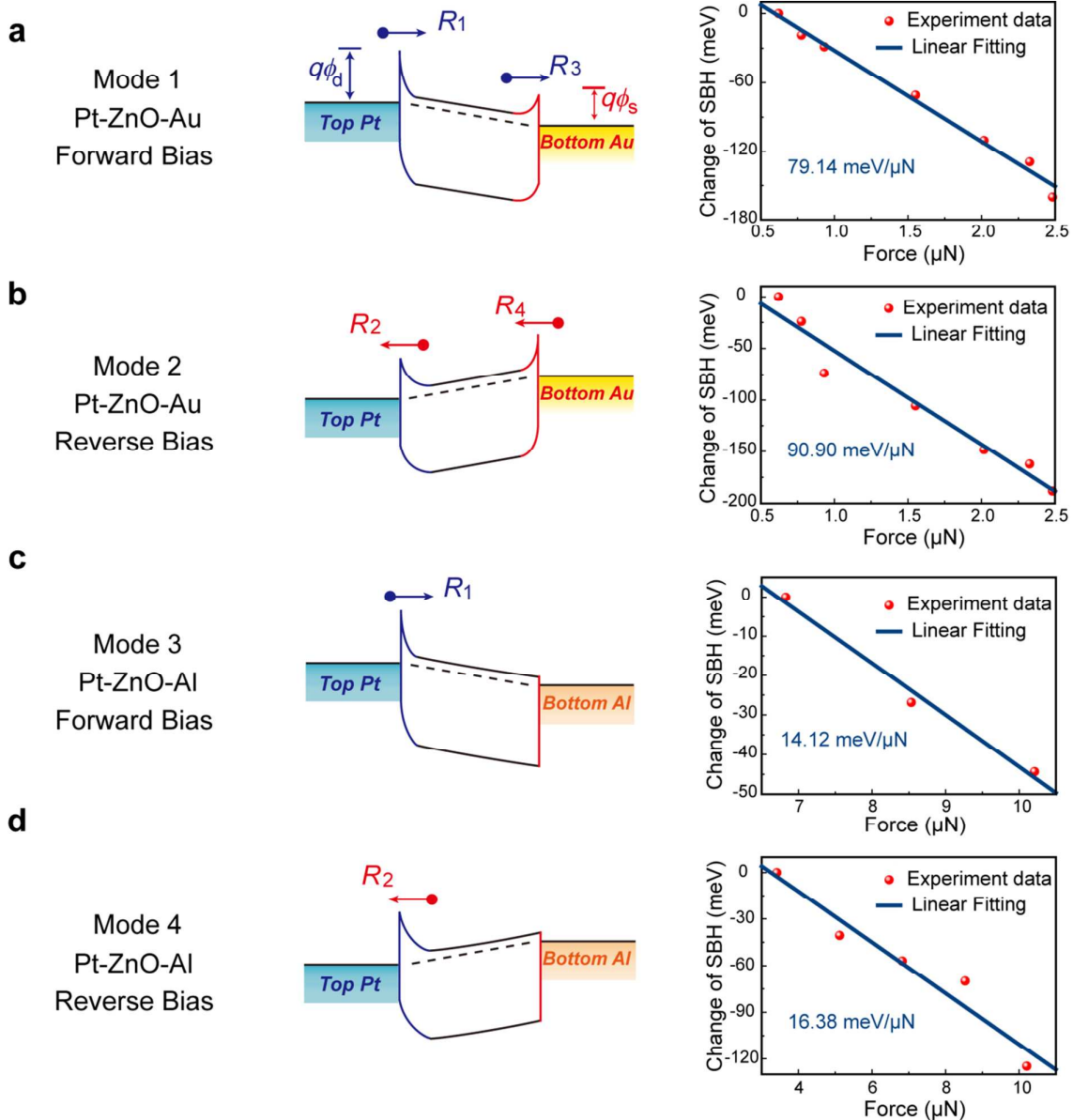
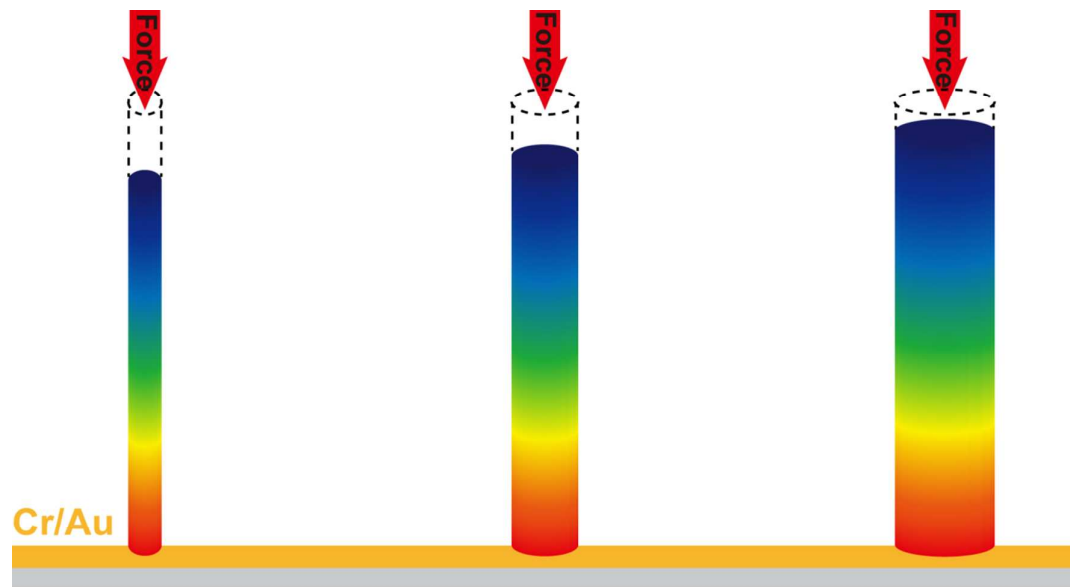


Figure S11. Force sensitivities of Schottky junctions to prove the bottom Schottky junction make a dominant role in regulating the ZnO twin nanoplatelet piezotronic transistor. (a, b) TNPT with bottom Au electrode in forward and reversed mode. (c, d) TNPT with bottom Al electrode in forward and reversed mode. R_1 and R_2 represent the effective barrier height of Pt-ZnO contact under forward and reversed bias respectively; while R_3 and R_4 represent the effective barrier height of Au-ZnO contact under forward and reversed bias, respectively.

4. Why we use the ‘Pressure sensitivity (meV/MPa)’, but not the ‘Force sensitivity (meV/nN)’?

Strain-gated piezotronic (photo)transistors based on nanomaterial with wurtzite structure (such as ZnO and GaN), operate through the modulation of local contact characteristics and charge carrier transport by strain-induced ionic polarization charges at the interfaces of metal-semiconductor contacts, which convert mechanical stimuli applied to the devices into local electronic controlling signals directly. Hence the force sensitivity, defined as $S = dSBH/dForce$, is one of the most important parameter. As shown in Figure S12, under same normal force, larger relative deformation would occur in slender NW and hence resulting in a larger Schottky barrier height change ΔSBH , if not considering the bending case of NW. It seems that the more slender the nanomaterial is, the larger force sensitivity it would have. The force sensitivity of NW seems to be dependent on the diameter for a same material. However, NW cluster consist of thousands of NWs usually used in functional nanodevices, which seems like a thick NW and hence with a ‘low’ force sensitivity.¹¹ It seems that the force sensitivity has limitation as a criterion of piezotronic transistor. Therefore, the pressure sensitivity, defined as $S=dSBH/dPressure$, is likely to be a more suitable parameter to estimate the performance of piezotronic transistor.



Force Sensitivity : $FS_{\text{left}} > FS_{\text{middle}} > FS_{\text{right}}$
Pressure Sensitivity : $PS_{\text{left}} = PS_{\text{middle}} = PS_{\text{right}}$

Figure S12. Pressure sensitivity.

Table S2. A comparison of strain sensing works.

Materials	Morphology	Sensor Type	Gauge factor	Response Time	Reference
ZnO	Twin nanoplatelet	Piezotronic sensor	$2.9\sim 9.4\times 10^9$	<5 ms	This Work
ZnO	Nanoplatelet	Piezotronic sensor	$\sim 1.5\times 10^7$	<5 ms	(1)
CdSe	NW, single	Piezotronic sensor	~ 1590		(15)
GaN	NW, single	Piezotronic sensor	~ 1126		(16)
GaN	NW, single	Piezotronic sensor		<5 ms	(17)
ZnO	NW, cluster	Piezotronic sensor	~ 784		(18)
ZnO	NW, cluster	Piezotronic sensor	$\sim 2\times 10^6$	150 ms	(10)
ZnO	NW, array	Piezotronic sensor	~ 1813		(19)
ZnO	NW, single	Piezotronic sensor		500 ms	(20)
ZnO	NB, single	Piezotronic sensor	~ 4036	120 ms	(21)
ZnO	NW, single	Piezotronic sensor	~ 1250	10 ms	(13)
ZnSnO ₃	NW, single	Piezotronic sensor	~ 3740		(22)
ZnO	NW, array	Piezotronic sensor	~ 1803	90 ms	(23)
Si	NW	Piezoresistive sensor	~ 200		
Carbon	Nanotube	Piezoresistive sensor	~ 1000		(24)
Carbon	Nanotube film	Piezoresistive sensor	0.06~0.82	14 ms	(25)
PDMS	Film	Piezoresistive sensor	550~5500		(26)
Polyurethane acrylate		Piezoresistive sensor	~ 11.45		(27)
Si/Ge and polyimide		Piezoresistive sensor		<0.1 s	(28)

5. Simulation of modulate effect of strain-induced piezo-potential on metal-ZnO Schottky barrier

To better explain the experimental results of ultrahigh pressure/strain sensitivity of TNPT and estimate the modulate effect of strain-induced piezo-potential on SBH of ZnO-metal contacts, we developed a 3D finite element (FE) model with COMSOL Multiphysics, as schematically shown in Figure S13. The previously reported two-terminal piezotronic transistors usually consist of a nano-/micro-wire or nanorod (such as ZnO, GaN and CdS) and metal electrodes. In this simulation setup, upon applying the normal tensile stress, accumulation of piezoelectric charges at both Schottky contacts induces the distribution of piezopotential (Figure S13a). Because of the orientation of the polar *c* axis in the as-synthesized ZnO NWs, positive piezopotential is induced at the top Schottky contact, which reduces the SBH and hence increases the transport conductance of the piezotronic transistor; while negative piezopotential is induced at bottom Schottky contact, which raises the SBH and hence decreases the transport conductance of the piezotronic transistor, as depicted by the schematic band diagrams in Figure S13b (inset). The strain-induced piezo-potentials at both Schottky contacts of the piezotronic transistor are opposite resulting in converse modulation on local SBHs of the metal-semiconductor Schottky contacts, thus limiting the pressure/strain sensitivity of the piezotronic transistor. It is further demonstrated by the theoretical calculated current-voltage curves of the nano-/micro wire based piezotronic transistor at different applied strains (Figure S13b), where the converse modulation trend was observed under opposite drain biases.

The theoretical simulation of a strained TNPT used in this work was investigated, as shown in Figure S13 (c and d). Due to the mirror symmetrical structure of ZnO twin nanoplatelet, piezo-potentials distribute along the ZnO twin nanoplatelet with negative piezoelectric polarization charges presenting at the top and bottom surfaces (Figure S13c), which can both

raise the SBHs and hence significantly weakens the transport conductance of a TNPT (Figure S13d), thus resulting in high pressure/strain sensitivity. The theoretically calculated current-voltage curves of a TNPT with different strains were shown in Figure S13d. By increasing the tensile strain, the transport conductance of the TNPT was decreased synchronously in both forward bias and reverse bias, which is in accordance with experimental data. Our simulation demonstrates high pressure/strain sensitivity and the dual Schottky junction synergistic modulation of TNPT, which can be applied as an active sensor for intelligent skin.

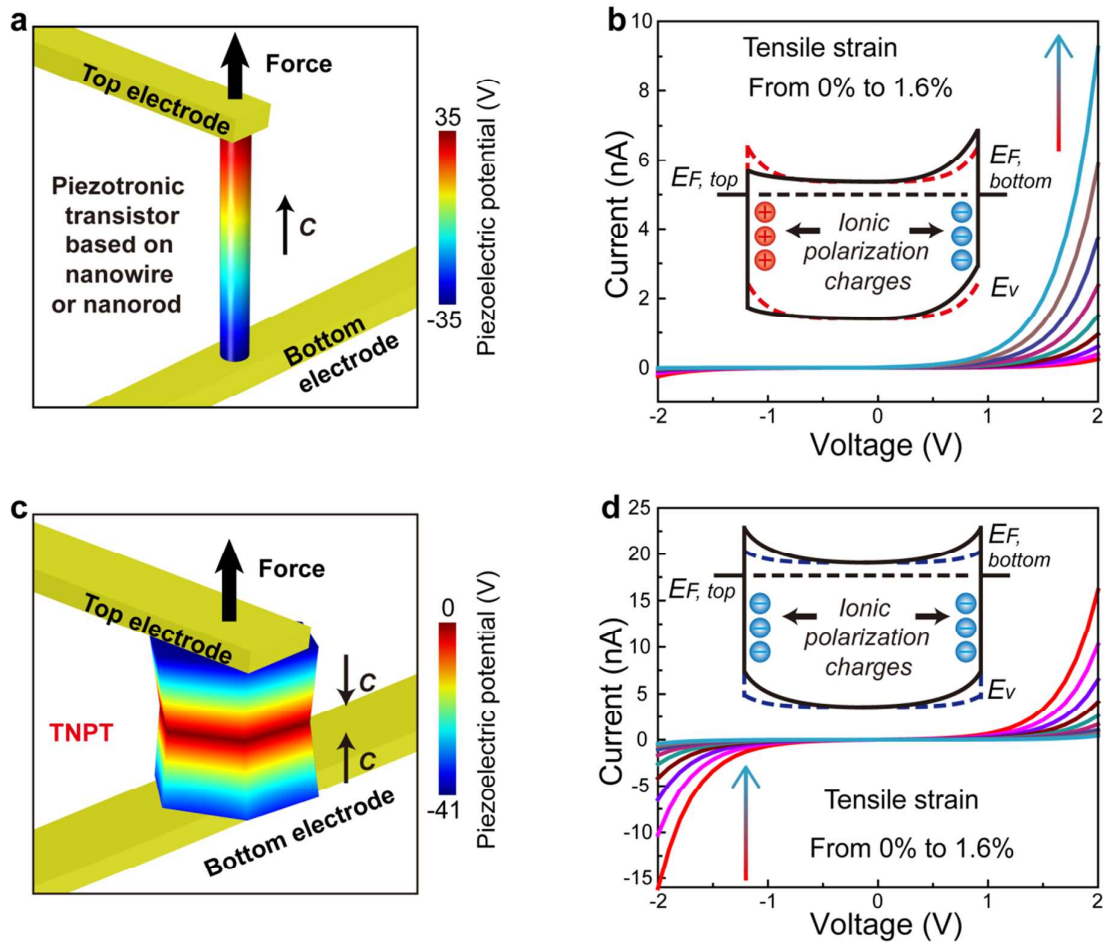


Figure S13 Simulation of modulate effect of tensile strain-induced piezo-potential on metal-ZnO Schottky barrier. a) Schematic of a piezotronic transistor based on traditional nano-/micro wire or nanorod with tensile strain, where the piezopotential controls the transport across the metal-semiconductor interface. Piezoelectric potential distributes within the ZnO nano-/micro wire under tensile strain of 0.001 is simulated by a finite-element analysis method. The diameter and length used for calculation is 600 nm and 5 μm respectively. b) Theoretical calculation of the current-voltage curves for the nano-/micro wire based piezotronic transistor at different applied strains. Inset: Schematic band diagram illustrating the change in SBH of the contact due to the modulation effect of strain-induced piezopotential. The original band edges at the contact for the piezotronic transistor without stress applied are shown as red dashed lines. The band edges bending at the contact for the device with stress applied are shown as black solid lines. c) Schematic of a TNPT with tensile strain, where the negative piezopotential controls the transport across the metal-semiconductor interfaces. Piezoelectric potential distributes within the ZnO twin nanoplatelet under tensile strain of 0.001 is simulated by a finite-element analysis method. The diameter and length used for calculation are 5 μm . d) Theoretical calculation the current-voltage curves for the TNPT at different applied strains. Inset: Schematic band diagram illustrating the change in SBH of the contact due to the modulation effect of strain-induced piezopotential. The original band edges at the contact for the TNPT without stress applied are shown as blue dashed lines. The band edges bending at the contact for the device with stress applied are shown as black solid lines.

6. Photoinduced response of the ZnO twin nanoplatelet based phototransistor.

The UV response of a ZnO twin nanoplatelet based phototransistor was investigated under 365 nm optical stimuli as summarized in Figure S14. The typical I_{ds} - V_{ds} characteristics shown in Figure S14a are nonlinear and ‘symmetric’ for small bias voltages, indicating a Schottky-like contact, and show an increase of drain current by several orders of magnitude as the device is illuminated. Upon illumination, the photo-generated holes migrate to the surface of ZnO twin nanoplatelets to discharge the negatively charged oxygen ions [$h^+ + O^{2-} = O_2(g)$], with the photo-generated electrons remaining, hence resulting in an increased charge carrier concentration and decreasing the width of the depletion layer.¹⁸ The accumulated electrons at the local metal-semiconductor interface reduce the Schottky barrier height (SBH), and therefore lead to the increased output currents as showed in Figure S14a. The response time of the UV PD array was investigated under constant UV illuminations at a biased voltage of 0.65 V as shown in Figure S14b. Upon straining (38.22 KPa), the response time was observed under illumination at an intensity of $4.5 \times 10^{-5} \text{ Wcm}^{-2}$, with a rise time of ~ 0.3 s and a fall time of ~ 0.4 s. We next explore the sensitivity of our photodetector, defined as $\Delta I = (I_{light} - I_{dark}) / I_{dark}$, where I_{light} and I_{dark} are the output current with and without illumination under a certain external strain respectively. The photosensitivity of the phototransistor under various illumination was derived and the results have been summarized in Figure S14c. It can be seen that the photosensitivity increased monotonically with the illumination intensity without saturations. The photosensitivity was calculated to be $\sim 1.2 \times 10^4\%$ under illumination with a power density of $4.5 \times 10^{-5} \text{ Wcm}^{-2}$. The other important figure of merit for a photodetector is its external photoresponsivity R defined as $R = (I_{light} - I_{dark}) / P_{illumination}$, where

$P_{illumination}$ is the illumination power on the phototransistor. Figure S14d shows the photoresponsivity R under various illumination intensity acquired at a bias voltage of $V=-0.65$ V. The largest R value reaches ~ 4967 AW^{-1} under illumination with a power density of 4×10^{-6} Wcm^{-2} .

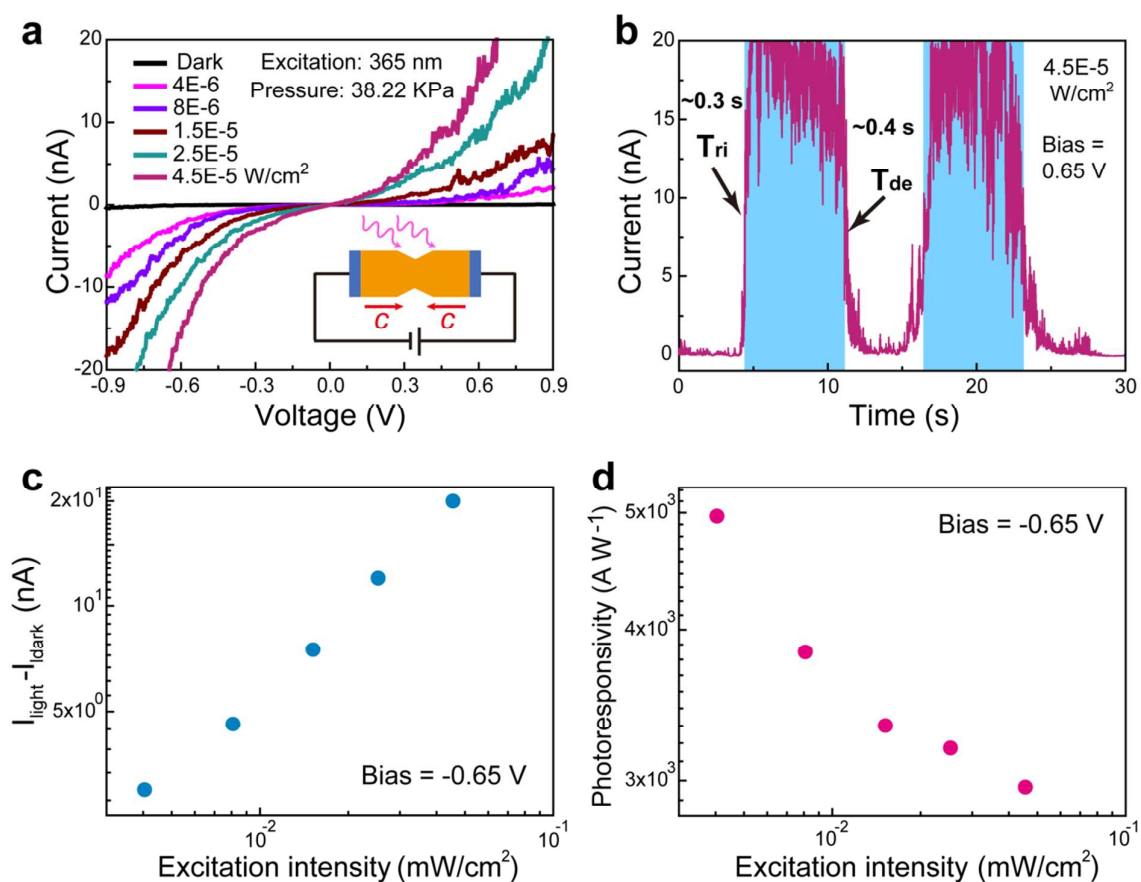


Figure S14. Photoreponse of the ZnO twin nanoplatelet based photodetector. a) Drain–source characteristic of the device in the dark and under different illumination intensities. The device operates as an enhancement-mode photodetector. Increasing illumination levels result in enhanced current due to electron–hole pair generation by light absorption in the direct bandgap of ZnO twin nanoplatelet. b) Time-resolved photoresponse of the device under 0.65 V and an illumination power density 4.5E-5 W/cm². The T_{rise} and T_{decay} are ~ 0.3 s and ~ 0.4 s respectively. Sensitivity (c) and Photoresponsivity (d) of the ZnO twin nanoplatelet photodetector, showing high sensitivity of the device.

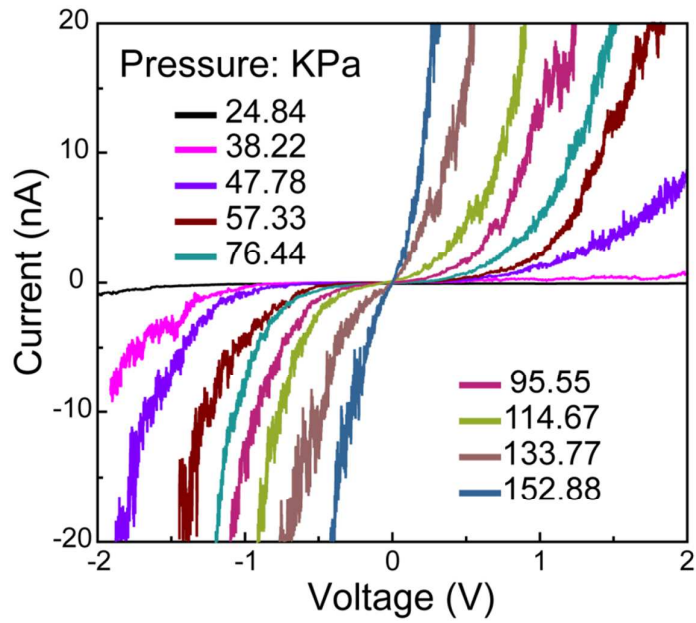


Figure S15. The modulation of carrier transport by pressure under opposite drain bias in a TNPT device, which shows characteristic of a piezotronic effect.

References

- 1 Liu, S.; Wang, L.; Feng, X.; Wang, Z.; Xu, Q.; Bai, S.; Qin, Y.; Wang, Z. L. Ultrasensitive 2D ZnO Piezotronic Transistor Array for High Resolution Tactile Imaging. *Adv. Mater.* **2017**, 1606346.
- 2 Crisler, D. F.; Cupal, J.J.; Moore, A. R. Dielectric Piezoelectric and Electromechanical Coupling Constants of ZnO Crystals. *A. R. Moore, Proc. IEEE* **1968**, *56*, 225-&.
- 3 Fan, H. J.; Lee, W.; Hauschild, R.; Alexe, M.; Le Rhun, G.; Scholz, R.; Dadgar, A.; Nielsch, K.; Kalt, H.; Krost, A.; Zacharias, M.; Gosele, U. Template-Assisted Large-Scale Ordered Arrays of ZnO Pillars for Optical and Piezoelectric Applications. *Small* **2006**, *2*, 561-568.
- 4 Scrymgeour, D. A.; Sounart, T. L.; Simmons, N. C.; Hsu, J. W. P. Polarity and Piezoelectric Response of Solution Grown Zinc Oxide Nanocrystals on Silver. *J. Appl. Phys.* **2007**, *101*, 014316.
- 5 Scrymgeour, D. A.; Hsu, J. W. P. Correlated Piezoelectric and Electrical Properties in Individual ZnO Nanorods. *Nano lett.* **2008**, *8*, 2204-2209.
- 6 Zhao, M. H.; Wang, Z. L.; Mao, S. X. Piezoelectric Characterization of Individual Zinc Oxide Nanobelt Probed by Piezoresponse Force Microscope. *Nano lett.* **2004**, *4*, 587-590.
- 7 Minary-Jolandan, M.; Bernal, R. A.; Kujanishvili, I.; Parpoil, V.; Espinosa, H. D. Individual GaN Nanowires Exhibit Strong Piezoelectricity in 3D. *Nano lett.* **2012**, *12*, 970-976.
- 8 Ke, T. Y.; Chen, H. A.; Sheu, H. S.; Yeh, J. W.; Lin, H. N.; Lee, C. Y.; Chiu, H. T. Sodium Niobate Nanowire and Its Piezoelectricity. *J. Phys. Chem. C* **2008**, *112*, 8827-8831.
- 9 Wang, J.; Stampfer, C.; Roman, C.; Ma, W. H.; Setter, N.; Hierold, C. Piezoresponse Force Microscopy on Doubly Clamped KNbO₃ Nanowires. *Appl. Phys. Lett.* **2008**, *93*, 223101.
- 10 Wang, Z. Y.; Suryavanshi, A. P.; Yu, M. F. Ferroelectric and Piezoelectric Behaviors of Individual Single Crystalline BaTiO₃ Nanowire under Direct Axial Electric Biasing. *Appl. Phys. Lett.* **2006**, *89*, 082903.
- 11 Wu, W. Z.; Wen, X. N.; Wang, Z. L. Taxel-Addressable Matrix of Vertical-Nanowire Piezotronic Transistors for Active and Adaptive Tactile Imaging. *Science* **2013**, *340*, 952-957.
- 12 Sze, S. M.; Ng, K. K. Physics of Semiconductor Devices. (John Wiley & sons, **2006**).
- 13 Liu, Y.; Zhang, Y.; Yang, Q.; Niu, S.; Wang, Z. L. Fundamental Theories of Piezotronics and Piezo-phototronics. *Nano Energy* **2015**, *14*, 257-275.
- 14 Zhou, J.; Fei, P.; Gu, Y. D.; Mai, W. J.; Gao, Y. F.; Yang, R.; Bao, G.; Wang, Z. L. Piezoelectric-Potential-Control led Polarity-Reversible Schottky Diodes and Switches of ZnO Wires. *Nano lett.* **2008**, *8*, 3035-3040.
- 15 Zhou, Y. S.; Wang, K.; Han, W. H.; Rai, S. C.; Zhang, Y.; Ding, Y.; Pan, C. F.; Zhang, F.; Zhou, W. L.; Wang, Z. L. Vertically Aligned CdSe Nanowire Arrays for Energy Harvesting and Piezotronic Devices. *ACS Nano* **2012**, *6*, 6478-6482.
- 16 Zhao, Z. F.; Pu, X.; Han, C. B.; Du, C. H.; Li, L. X.; Jiang, C. Y.; Hu, W. G.; Wang, Z. L. Piezotronic Effect in Polarity-Controlled GaN Nanowires. *ACS Nano* **2015**, *9*, 8578-8583.
- 17 Zhou, Y. S.; Hinchet, R.; Yang, Y.; Ardila, G.; Songmuang, R.; Zhang, F.; Zhang, Y.; Han, W. H.; Pradel, K.; Montes, L.; Mouis, M.; Wang, Z. L. Nano-Newton Transverse Force Sensor Using a Vertical GaN Nanowire based on the Piezotronic Effect. *Adv. Mater.* **2013**, *25*, 883-888.
- 18 Han, X.; Du, W. M.; Yu, R. M.; Pan, C. F.; Wang, Z. L. Piezo-Phototronic Enhanced UV Sensing based on a Nanowire Photodetector Array. *Adv. Mater.* **2015**, *27*, 7963-7969.
- 19 Zhang, W. G.; Zhu, R.; Nguyen, V.; Yang, R. S. Highly Sensitive and Flexible Strain Sensors based on Vertical Zinc Oxide Nanowire Arrays. *Sens. Actuators A Phys.* **2014**, *205*, 164-169.

- 20 Yang, Y.; Qi, J. J.; Gu, Y. S.; Wang, X. Q.; Zhang, Y. Piezotronic Strain Sensor based on Single Bridged ZnO Wires. *Phys. Status Solidi RRL Rapid Res. Lett.* **2009**, *3*, 269–271.
- 21 Zhang, Z.; Liao, Q.L.; Zhang, X.H.; Zhang, G.J.; Li, P.F.; Lu, S.N.; Liu, S.; Zhang, Y.. Highly Efficient Piezotronic Strain Sensors with Symmetrical Schottky Contacts on the Monopolar Surface of ZnO Nanobelts. *Nanoscale* **2015**, *7*, 1796-1801.
- 22 Wu, J. M.; Chen, C. Y.; Zhang, Y.; Chen, K. H.; Yang, Y.; Hu, Y. F.; He, J. H.; Wang, Z. L. Ultrahigh Sensitive Piezotronic Strain Sensors based on a ZnSnO₃ Nanowire/Microwire. *ACS nano* **2012**, *6*, 4369-4374.
- 23 Pan, C. F.; Dong, L.; Zhu, G.; Niu, S. M.; Yu, R. M.; Yang, Q.; Liu, Y.; Wang, Z. L. High-Resolution Electroluminescent Imaging of Pressure Distribution Using a Piezoelectric Nanowire LED Array. *Nat. Photon.* **2013**, *7*, 752-758.
- 24 Cao, J.; Wang, Q.; Dai, H. J. Electromechanical Properties of Metallic, Quasimetallic, and Semiconducting Carbon Nanotubes under Stretching. *Phys. Rev. Lett.* **2003**, *90*, 157601.
- 25 Yamada, T.; Hayamizu, Y.; Yamamoto, Y.; Yomogida, Y.; Izadi-Najafabadi, A.; Futaba, D. N.; Hata, K. A. Stretchable Carbon Nanotube Strain Sensor for Human-Motion Detection. *Nat. Nanotechnol.* 2011, *6*, 296-301.
- 26 Mannsfeld, S. C. B.; Tee, B. C. K.; Stoltenberg, R. M.; Chen, C. V.; Barman, S.; Muir, B. V. O.; Sokolov, A. N.; Reese, C.; Bao, Z. N. Highly Sensitive Flexible Pressure Sensors with Microstructured Rubber Dielectric Layers. *Nat. Mater.* **2010**, *9*, 859-864.
- 27 Pang, C.; Lee, G. Y.; Kim, T. I.; Kim, S. M.; Kim, H. N.; Ahn, S. H.; Suh, K. Y. A Flexible and Highly Sensitive Strain-Gauge Sensor Using Reversible Interlocking of Nanofibres. *Nat. Mater.* **2012**, *11*, 795-801.
- 28 Takei, K.; Takahashi, T.; Ho, J. C.; Ko, H.; Gillies, A. G.; Leu, P. W.; Fearing, R. S.; Javey, A. Nanowire Active-Matrix Circuitry for Low-Voltage Macroscale Artificial Skin. *Nat. Mater.* **2010**, *9*, 821-826.